Mathematical Biosciences and Engineering

http://www.aimspress.com/journal/MBE

MBE, 16(5): 3841–3863.
DOI: 10.3934/mbe.2019190
Received: 18 January 2019
Accepted: 19 April 2019
Published: 29 April 2019

Research article

A mathematical model to study the 2014–2015 large-scale dengue epidemics in Kaohsiung and Tainan cities in Taiwan, China

Salihu Sabiu Musa[1], Shi Zhao[1,2], Hei-Shen Chan[1], Zhen Jin[3,4,5,*] and Daihai He[1,*]

[1] Department of Applied Mathematics, Hong Kong Polytechnic University, Hong Kong, China

[2] School of Nursing, Hong Kong Polytechnic University, Hong Kong, China

[3] Complex System Research Center, Shanxi University, Taiyuan 030006, Shanxi, China

[4] Shanxi Key Laboratory of Mathematical Techniques and Big Data Analysis on Disease Control and Prevention, Shanxi University, Taiyuan 030006, Shanxi, China

[5] Key Laboratory of Computational Intelligence and Chinese Information, Processing of Ministry of Education, Taiyuan 030006, China

* **Correspondence:** Email: daihai.he@polyu.edu.hk, jinzhn@263.net.

Abstract: Dengue virus (DENV) infection is endemic in many places of the tropical and subtropical regions, which poses serious public health threat globally. We develop and analyze a mathematical model to study the transmission dynamics of the dengue epidemics. Our qualitative analyzes show that the model has two equilibria, namely the disease-free equilibrium (DFE) which is locally asymptotically stable when the basic reproduction number ($\mathcal{R}_0$) is less than one and unstable if $\mathcal{R}_0 > 1$, and endemic equilibrium (EE) which is globally asymptotically stable when $\mathcal{R}_0 > 1$. Further analyzes reveals that the model exhibit the phenomena of backward bifurcation (BB) (a situation where a stable DFE co-exists with a stable EE even when the $\mathcal{R}_0 < 1$), which makes the disease control more difficult. The model is applied to the real dengue epidemic data in Kaohsiung and Tainan cities in Taiwan, China to evaluate the fitting performance. We propose two reconstruction approaches to estimate the time-dependent $\mathcal{R}_0$, and we find a consistent fitting results and equivalent goodness-of-fit. Our findings highlight the similarity of the dengue outbreaks in the two cities. We find that despite the proximity in Kaohsiung and Tainan cities, the estimated transmission rates are neither completely synchronized, nor periodically in-phase perfectly in the two cities. We also show the time lags between the seasonal waves in the two cities likely occurred. It is further shown via sensitivity analysis result that proper sanitation of the mosquito breeding sites and avoiding the mosquito bites are the key control measures to future dengue outbreaks in Taiwan.

Keywords: Dengue virus; mathematical modelling; Taiwan; stability analysis; backward bifurcation

1. Introduction

Dengue virus (DENV), a *flavivirus* primarily transmitted to human via a bites of an infected mosquitoes of the genus *Aedes* (i.e., *Aedes aegypti* or *Aedes albopictus*) [1, 2, 3, 4, 5, 6, 7, 8, 9, 10]. This species is capable of transmitting other mosquito-borne diseases such as Chikungunya, Zika, Yellow fever [3, 11, 12, 13, 14]. The DENV is endemic in at least 100 countries in the tropical and subtropical regions of the world, with nearly 4 billion people at risk [7, 15]. It is second to malaria amongst the deadly mosquito-borne diseases with fast-spreading ability [7], with an estimate of 390 million new infections of which about 96 million are clinical, up to 1 million are severe cases (i.e., dengue hemorrhagic fever/dengue shock syndrome also known as DHF/DSS), and more than 20 thousand deaths every year globally [6, 7, 16]. The DHF/DSS have a high mortality risk with death occurring within 24hrs after the onset of shock [17, 18, 19]).

The DENV are of four serotypes (i.e., DENV-1, DENV-2, DENV-3 and DENV-4) with low cross-immunity among each other which can result in secondary infection after an infection with one serotype has happened [7]. An individual infected with one serotype can be infected with different serotypes about a half year later [3], yet there is no proof of reinfection with the same serotype. DEN infection of all serotypes can cause three distinct syndromes: classic dengue fever, DHF and DSS [3].

The epidemiological cycle occurs as follows. Female *Aedes aegypti* mosquitoes are infected by the blood meal from biting an infectious human during the viremic stage of the infection. After a period of time called the extrinsic incubation period (EIP), the mosquitoes become infectious [20]. The range of the extrinsic incubation period lies between 4 to 10 days [20]. The infected mosquito does not have immunity and can transmit the virus throughout its lifespan [3, 7, 20]. An infectious mosquito can transmit the virus to a susceptible individual via bites [21], after a period of time called the intrinsic incubation period (IIP), which varies from 4 to 7 days [20], the virus can evolve from classical dengue fever to the secondary cases of dengue infection which may lead to DHF or DSS [17]. The manifestation of the symptoms varies between 3 to 7 days [3], which corresponds roughly to the infectious period. Thereafter, the individual develops the life-long immunity against the same serotype of the virus [3].

The prevention against DENV is limited to controlling mechanisms applied on the mosquito, because the vaccine is not yet available (even though there is a vaccine called dengvaxia, which is still under clinical trial, released by Sanofi Pasteur in 2015 which was approved by morethan 10 countries [7, 22]. The vaccine efficacy varies by the serotypes of the DENV (i.e., 54.7 % for DENV-1, 43.0 % for DENV-2, 71.6 % for DENV-3, and 76.9 % for DENV-4 [7, 23]). To describe the overall transmission dynamics of the DENV, we developed a mathematical model that takes into account the female adult mosquito coupled with the human population to analyses and explain the transmission dynamics of the DENV epidemics in Taiwan in 2014-2015.

A number of mathematical modeling studies have been carried out to gain insight into the DENV transmission dynamics in human and/or mosquito populations [3, 4, 5, 6, 11, 24, 25]. Garba *et al.* [6] developed a deterministic model for the DENV transmission within human and mosquito populations, and extended the model to incorporate an imperfect vaccine against the virus, and find that both models exhibited backward bifurcation phenomenon, and the courses have been explained in detail by Gumel [26]. Yang and Ferreiri [3] proposed a model to describe the transmission dynamics of the DENV in human and mosquito populations, they incorporated aquatic stages (i.e., eggs, larvae, pupae) in

the mosquito population, and calculated the basic reproduction number to be less than one (which indicate that the disease can dies out in time). Yang *et al.* [24] designed a simple model in order to assess the effect of temperature on the population of the mosquito by using the temperature controlled experiments. Yang *et al.* [25] extended Yang *et al.* [24] by including human compartments and updated most of the parameters to assess the effect of temperature on the risk of the DENV outbreaks. Yang [5] developed and analyzed a model encompassing four quiescence stages of the mosquito, and used the model to assess the influence of the quiescent eggs on the transmission dynamics of the mosquito.

In the current study, we focus on the design and analysis of a model, which extends some of the aforementioned studies, for assessing the transmission dynamics of the DENV in human and mosquito populations. Our model includes both the human and mosquito populations, and incorporates asymptomatic (A_h) and severe cases (those with DHF/DSS) of the DENV infection (I_{h_2}) in human population. We performed model fitting by using the plug-and-play inference framework for the human population, and our results contribute to better understanding of the transmission dynamics of the DENV epidemics in Taiwan in 2014-15 and provide useful guidelines for the design of control strategies in the future.

The paper is organized as follows. The model is formulated in section 2 and analyzed in section 3. Sensitivity analysis results of the full model is also given in section 4. Finally numerical analysis of the human only sub-model is performed with a plug-and-play inference framework in section 5.

2. Model formulation

2.1. Dengue epidemic model

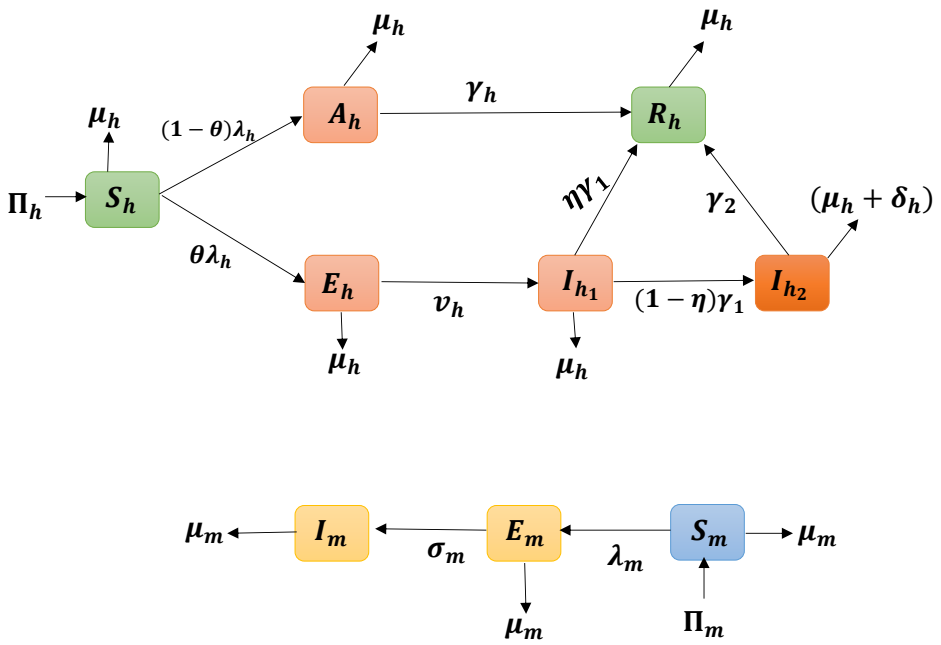

Figure 1. Schematic diagram of the model (2.1).

The total human population at time t, denoted by $N_h(t)$, is divided into six compartments of susceptible, $S_h(t)$, exposed (infected but not infectious individuals that can progress to I_{h1} class), $E_h(t)$, asymptomatically infected, $A_h(t)$ (i.e., expose individuals that can progress and becomes infectious without showing any clinical symptoms, which are lumped together for computational conveniences), symptomatically infected, $I_{h_1}(t)$, symptomatically infected with severe DENV (DHF/DSS), $I_{h_2}(t)$, and recovered, $R_h(t)$, humans. Hence,

$$N_h(t) = S_h(t) + E_h(t) + A_h(t) + I_{h_1}(t) + I_{h_2}(t) + R_h(t).$$

The total mosquito population at time t, denoted by $N_m(t)$, is split into susceptible $S_m(t)$, exposed (infected but not infectious mosquitoes) $E_m(t)$ and symptomatic (infectious mosquitoes) $I_m(t)$ classes. Hence,

$$N_m(t) = S_m(t) + E_m(t) + I_m(t).$$

The model for the DENV transmission in the human and mosquito populations is given by the following deterministic ordinary differential equations (ODE) systems (2.1). The flow diagram of the model (2.1) is depicted in Figure 1. The state variables and parameters of the model are described in Tables 1 and 2, respectively.

$$\begin{aligned}
\frac{dS_h}{dt} &= \Pi_h - \lambda_h S_h - \mu_h S_h,\\
\frac{dE_h}{dt} &= \theta\lambda_h S_h - (\nu_h + \mu_h)E_h,\\
\frac{dA_h}{dt} &= (1-\theta)\lambda_h S_h - (\gamma_h + \mu_h)A_h,\\
\frac{dI_{h_1}}{dt} &= \nu_h E_h - (\gamma_1 + \mu_h)I_{h_1},\\
\frac{dI_{h_2}}{dt} &= (1-\eta)\gamma_1 I_{h_1} - (\delta_h + \gamma_2 + \mu_h)I_{h_2},\\
\frac{dR_h}{dt} &= \eta\gamma_1 I_{h_1} + \gamma_2 I_{h_2} + \gamma_h A_h - \mu_h R_h,\\
\frac{dS_m}{dt} &= \Pi_m - \lambda_m S_m - \mu_m S_m,\\
\frac{dE_m}{dt} &= \lambda_m S_m - (\sigma_m + \mu_m)E_m,\\
\frac{dI_m}{dt} &= \sigma_m E_m - \mu_m I_m.
\end{aligned} \tag{2.1}$$

Here, the infection rate for humans (λ_h) and vectors (λ_m) are given by

$$\lambda_h = \frac{ab\beta_h I_m}{N_h}, \text{ and } \lambda_m = \frac{ab\beta_m(A_h + I_{h_1} + I_{h_2})}{N_h}. \tag{2.2}$$

In model (2.1), Π_h is the recruitment rate for human by birth, λ_h is the infection rate of susceptible human from infectious mosquitoes, where a is the mosquito biting rate, b is the maximum number of bites a human can receive per unit time, β_h is the transmission probability from infected mosquitoes to

the susceptible humans while β_m is transmission probability from an infectious humans to the susceptible mosquitoes per bite, and μ_h is the natural death rate of human. The term θ is the symptomatic ratio, and $(1-\theta)$ remains the fraction of asymptomatic ratio. The parameter v_h measures the rate at which an individuals in the E_h class develop a primary clinical symptoms of the virus, while η is a fraction of humans who will not get a severe DENV, δ_h accounts for the disease-induced death rate of humans from the I_{h_2} class, and $\gamma_i (i = 0, 1, 2)$ measures the rate of recovery of individual from A_h, I_{h_1}, and I_{h_2}, respectively.

The susceptible adult mosquitoes acquire the DENV at a rate λ_m, this population is decreased by natural death at a rate μ_m. Finally, σ_m is a progression rate of the DENV from the $E_m(t)$ class to the $I_m(t)$. It is also worth stating that the model (2.1) accounts for the conservation law of mosquito bites. Thus, the infection rates, λ_h and λ_m, are normalized by the total host population, that is $N_h(t)$ [27].

2.2. Basic properties

The basic properties of the model (2.1) will now be explored. Consider the following equations for the rate of change of the total human $N_h'(t)$ and mosquito $N_m'(t)$ populations

$$N_h'(t) = \frac{dN_h}{dt} = \Pi_h - \mu_h N_h - \delta_h I_{h_2} \leqslant \Pi_h - \mu_h N_h, \tag{2.3}$$

and

$$N_m'(t) = \frac{dN_m}{dt} = \Pi_m - \mu_m N_m, \tag{2.4}$$

here, the prime, $'$, represent a differentiation with respect to time, t.

Table 1. Descriptions of compartmental classes in the model (2.1).

Variable	Interpretation
$N_h(t)$	Total population of humans
$S_h(t)$	Population of susceptible humans
$E_h(t)$	Population of humans exposed to DENV
$A_h(t)$	Population of asymptomatic humans
$I_{h_1}(t)$	Population of humans with clinical symptoms of the DENV
$I_{h_2}(t)$	Population of humans with severe clinical symptoms of the DENV
$R_h(t)$	Population of humans recovered from the DENV
$N_m(t)$	Total population of adult female mosquitoes
$S_m(t)$	population of susceptible adult mosquitoes
$E_m(t)$	population of exposed adult mosquitoes
$I_m(t)$	population of infectious adult mosquitoes

Furthermore, consider the region,

$$\Omega = \left\{(S_h, E_h, A_h, I_{h_1}, I_{h_2}, R_h, S_m, E_m, I_m) \in \mathbb{R}^9_+ : N_h \leqslant \frac{\Pi_h}{\mu_h}, N_m \leqslant \frac{\Pi_m}{\mu_m}\right\}.$$

It can be shown by solving for N_h and N_m in Eqs (2.3)-(2.4) so that all solutions of the system starting in the region Ω will remain in Ω for all time t with $t \geqslant 0$. Thus, the region Ω is positively-invariant, and it is sufficient to consider solutions restricted in Ω. In this region, the usual existence, uniqueness and continuation results hold for the system (2.1) [28, 29].

Table 2. Description of the parameters in the model (2.1).

Parameter	Interpretation / Description
Π_h/Π_m	Recruitment rate of humans/mosquitoes
μ_h	Natural death rate of humans
μ_m	Death rate of female adult mosquitoes
β_h	Transmission probability from infectious mosquitoes to susceptible humans
β_m	Transmission probability from infectious humans to susceptible mosquitoes
a	Mosquito biting rate
b	Maximum number of bites a human can receive per unit time
θ	Fraction of infected humans that are exposed
v_h	Progression rate of exposed humans to infectious humans with clinical symptoms
η	Fraction of infectious humans that will not get a severe symptom
γ_h, γ_1, γ_2	Recovery rate of infectious humans from A_h, I_{h_1}, I_{h_2}, respectively
δ_h	Disease-induced death rate of humans
σ_m	Progression rate of exposed mosquitoes to the infectious mosquitoes
ρ	Reporting rate to actual case ratio
m	Average mosquito to human ratio

3. Mathematical analysis

3.1. Disease-free equilibrium and its stability

The disease-free equilibrium (DFE) of the model (2.1) obtained at steady state is given by

$$E^0 = \left(S_h^0, E_h^0, A_h^0, I_{h1}^0, I_{h2}^0, R_h^0, S_m^0, E_m^0, I_m^0\right) = \left(\frac{\Pi_h}{\mu_h}, 0, 0, 0, 0, 0, \frac{\Pi_m}{\mu_m}, 0, 0\right).$$

Using the next generation matrix method [30], we obtained the associated reproduction number of the model (2.1), denoted by $\mathcal{R}_0 = \rho(FV^{-1})$. The term ρ represents the function to find the spectral radius of the next generation matrix, $\mathbf{G} = FV^{-1}$. The matrices F (for the new infection terms) and V (for the remaining transition terms), associated with the model (2.1), are given by

$$F = \begin{bmatrix} 0 & 0 & 0 & 0 & 0 & \theta\, ab\beta_h \\ 0 & 0 & 0 & 0 & 0 & (1-\theta)\, ab\beta_h \\ 0 & 0 & 0 & 0 & 0 & 0 \\ 0 & 0 & 0 & 0 & 0 & 0 \\ 0 & \frac{ab\beta_m S_m^0}{N_h} & \frac{ab\beta_m S_m^0}{N_h} & \frac{ab\beta_m S_m^0}{N_h} & 0 & 0 \\ 0 & 0 & 0 & 0 & 0 & 0 \end{bmatrix}, \tag{3.1}$$

$$V = \begin{bmatrix} n_1 & 0 & 0 & 0 & 0 & 0 \\ 0 & n_2 & 0 & 0 & 0 & 0 \\ -v_h & 0 & n_3 & 0 & 0 & 0 \\ 0 & 0 & -(1-\eta)\,\gamma_1 & n_4 & 0 & 0 \\ 0 & 0 & 0 & 0 & n_5 & 0 \\ 0 & 0 & 0 & 0 & -\sigma_m & \mu_m \end{bmatrix}, \tag{3.2}$$

where $n_1 = v_h + \mu_h$, $n_2 = \gamma_h + \mu_h$, $n_3 = \gamma_1 + \mu_h$, $n_4 = \delta_h + \gamma_2 + \mu_h$, and $n_5 = \sigma_m + \mu_m$. Therefore, the basic reproduction number, $\mathcal{R}_0$, is given by

$$\mathcal{R}_0 = \mathcal{R}_h \cdot \mathcal{R}_m, \tag{3.3}$$

where

$$\mathcal{R}_h = \sqrt{\frac{ab\beta_h\mu_h}{\Pi_h} \cdot \left[\frac{\theta v_h}{n_1 n_3} + \frac{\theta(1-\eta)\gamma_1 v_h}{n_1 n_3 n_4} + \frac{(1-\theta)}{n_2}\right]}, \tag{3.4}$$

and

$$\mathcal{R}_m = \sqrt{\frac{ab\beta_m\sigma_m S_m^0}{n_5\mu_m}}. \tag{3.5}$$

$\mathcal{R}_0$ **interpretation:** The threshold quantity $\mathcal{R}_0$ is ecologically and epidemiologically interpreted as follows.

i. $\frac{ab\beta_h}{N_h}$ accounts for the number of new infected human hosts caused by an infected mosquito over its expected infectious period,
ii. $\frac{v_h}{n_1}$ is the probability that an exposed human survives the exposed stage and move to the infectious stage, I_{h_1},
iii. $\frac{1}{n_3}$ is the average duration in the infectious stage,
iv. $\frac{(1-\eta)\gamma_1}{n_4}$ is the probability that an infectious human survives the infectious stage (including severe stage of the DENV) and move to the recovered class,
v. $\frac{(1-\theta)}{n_2}$ is the probability that an infected human move to the asymptomatic class,
vi. $ab\beta_m \frac{\sigma_m}{n_5}\frac{S_m^0}{\mu_m}$ accounts for the possible number of new infected mosquito caused by an infected human hosts over its exposed infectious period.

Table 3. Values and ranges of the parameters of the model (2.1).

Parameter	Baseline [Range]	Units	Source
Π_h	2.5 [1, 5]	person day^{-1}	[6]
Π_m	5000 [1000, 6000]	Day^{-1}	estimated from [6]
μ_h	3.9×10^{-5} [3.6×10^{-5}, 4.0×10^{-5}]	Day^{-1}	[12]
μ_m	0.05714 [0.01, 0.1]	Day^{-1}	[11]
β_h	0.75 [0.1, 0.95]	Day^{-1}	[6]
β_m	0.75 [0.1, 0.95]	Day^{-1}	[6]
a	0.4997 [0.1, 1]	Day^{-1}	[13, 14]
b	0.4 [0.1, 1]	Day^{-1}	[13]
θ	0.18 [0.1, 0.6]	Dimensionless	[31]
ν_h	0.0666 [0, 1]	Day^{-1}	[6, 32]
η	0.1 [0.05, 0.15]	Dimensionless	[19, 33]
γ_h	0.1428 [0.1, 0.2]	Day^{-1}	[13]
γ_1	0.2 [0.1428, 0.3]	Day^{-1}	[13]
γ_2	0.05 [0.0333, 0.07143]	Day^{-1}	[13]
δ_h	10^{-3} [10^{-4}, 2×10^{-3}]	Day^{-1}	[6]
σ_m	0.5 [0, 1]	Day^{-1}	[6]
m	10 [1, 20]	Dimensionless	assumed

The theorem 3.1 below follows the Theorem 2 of Ref [30].

Theorem 3.1. *The DFE, E^0, of the model* (2.1)*, is locally-asymptotically stable (LAS) in Ω if $\mathcal{R}_0 < 1$, but unstable if $\mathcal{R}_0 > 1$.*

3.2. Existence of endemic equilibrium and backward bifurcation

3.2.1. Endemic equilibrium and backward bifurcation

The endemic equilibrium (EE) for the system (2.1), which is

$$E^* = (S_h^*, E_h^*, A_h^*, I_{h1}^*, I_{h2}^*, R_h^*, S_m^*, E_m^*, I_m^*),$$

in terms of the forces of infection, λ_h^* and λ_m^*, is given by

$$\begin{aligned}
&S_h^* = \frac{\Pi_h}{\lambda_h + \mu_h}, \quad E_h^* = \frac{\theta\lambda_h\Pi_h}{n_1(\lambda_h + \mu_h)}, \quad A_h^* = \frac{(1-\theta)\lambda_h\Pi_h}{n_2(\lambda_h + \mu_h)}, \quad I_{h1}^* = \frac{\nu_h\theta\lambda_h\Pi_h}{n_1n_3(\lambda_h + \mu_h)},\\
&I_{h2}^* = \frac{(1-\eta)\gamma_1\nu_h\theta\lambda_h\Pi_h}{n_1n_3n_4(\lambda_h + \mu_h)}, \quad R_h^* = \frac{\Pi_h\lambda_h}{\mu_h(\lambda_h + \mu_h)}\left(\frac{(1-\theta)\gamma_h}{n_2} + \frac{\eta\gamma_1\nu_h\theta}{n_1n_3} + \frac{\gamma_1\gamma_2(1-\eta)\nu_h\theta}{n_1n_3n_4}\right),\\
&S_m^* = \frac{\Pi_m}{\lambda_m + \mu_m}, \quad E_m^* = \frac{\Pi_m\lambda_m}{n_5(\lambda_m + \mu_m)} \quad \textit{and} \quad I_m^* = \frac{\sigma_m\Pi_m\lambda_m}{n_5\mu_m(\lambda_m + \mu_m)}.
\end{aligned} \tag{3.6}$$

Substituting the above equilibrium points (equation (3.6)) into equation (2.2), we have

$$A\lambda_h^2 + B\lambda_h + C = 0, \tag{3.7}$$

where
$A = \Pi_h(\sigma_m + \mu_m)\mu_m(-ab\beta_m\mu_h\theta v_h n_2 n_4 - ab\beta_m\mu_h\gamma_1\theta v_h n_2 + ab\beta_m\mu_h\gamma_1\theta v_h n_2\eta - ab\beta_m\mu_h(1-\theta)n_1 n_3 n_4 - \mu_m\theta\mu_h n_2 n_3 n_4 - \mu_m(1-\theta)\mu_h n_1 n_3 n_4 - \mu_m\theta v_h\mu_h n_2 n_4 - \mu_m\gamma_1\theta v_h\mu_h n_2 + \mu_m\gamma_1\theta v_h\mu_h n_2\eta - \mu_m\gamma_h(1-\theta)n_1 n_3 n_4 - \mu_m\eta\gamma_1 v_h\theta n_2 n_4 - \mu_m\gamma_1\gamma_2 v_h\theta n_2 + \mu_m\gamma_1\gamma_2 v_h\theta n_2\eta)(-\theta\mu_h n_2 n_3 n_4 - (1-\theta)\mu_h n_1 n_3 n_4 - \theta v_h\mu_h n_2 n_4 - \gamma_1\theta v_h\mu_h n_2 + \gamma_1\theta v_h\mu_h n_2\eta - \gamma_h(1-\theta)n_1 n_3 n_4 - \eta\gamma_1 v_h\theta n_2 n_4 - \gamma_1\gamma_2 v_h\theta n_2 + \gamma_1\gamma_2 v_h\theta n_2\eta)$,
$B = n_4 n_2 n_1\mu_h(-\mu_m(\sigma_m + \mu_m)[((((-2n_3 - 2v_h)n_4 + 2\gamma_1 v_h(-1+\eta))n_2 + 2n_1 n_3 n_4)\mu_h - 2v_h(n_4\eta - \gamma_2(-1+\eta))\gamma_1 n_2 + 2\gamma_h n_1 n_3 n_4)\theta - 2n_1 n_3 n_4(\mu_h + \gamma_h))\mu_m + a(((-n_4 + \gamma_1(-1+\eta))v_h n_2 + n_1 n_3 n_4)\theta - n_1 n_3 n_4)\mu_h b\beta_m]\Pi_h + a^2\sigma_m(((-n_4 + \gamma_1(-1+\eta))v_h n_2 + n_1 n_3 n_4)\theta - n_1 n_3 n_4)\mu_h\Pi_m b^2\beta_m\beta_h)n_3$, and $C = (1 - \mathcal{R}_0^2)$.

Therefore, one can obtain the positive EE of the model (2.1) by simplifying the quadratic equation (3.7), and substituting only the positive values of the λ_h into the EE points. The occurrence of the quadratic equation (3.7) shows that the backward bifurcation (BB) for the model (2.1) exists.

Hence, the following Theorem 3.2 is established.

Theorem 3.2. *The model (2.1) has*

i) a EE if $C < 0 \Leftrightarrow \mathcal{R}_0 > 1$*;*
ii) a unique EE if $B < 0$ *and* $C = 0$ *or* $B^2 - 4AB = 0$*;*
iii) two EEs if $B < 0$, $C > 0$ *and* $B^2 - 4AC > 0$*; or*
iv) no EE otherwise.

The existence of the phenomenon of the BB in the model (2.1) highlights a co-existence between a stable disease free-equilibrium (DFE) and a stable endemic equilibrium (EE) even if the basic reproduction number ($\mathcal{R}_0$) is less than unity, this makes the disease control more difficult. Furthermore, the disease eradication would no longer depends on the basic concept of $\mathcal{R}_0$, i.e., when $\mathcal{R}_0 < 1$, the disease dies out in time; and while $\mathcal{R}_0 > 1$, the disease persists in the community. Although the BB has been firstly shown to exist in the DENV from the work of Garba *et al.* [6] and its courses has been explained extensively by Gumel [26]. In this study, our analysis suggests that the BB can be removed if the $\mathcal{R}_0$ can be equal to one (i.e., $\mathcal{R}_0 = 1$), so that equation (3.7) will be $A\lambda_h + B = 0$ which is linear equation.

3.2.2. Global stability analysis of the endemic equilibrium

The following Theorem 3.3 is claimed.

Theorem 3.3. *The endemic equilibrium (EE),* E^**, is globally-asymptotically stable (GAS) in* Ω *when* $\mathcal{R}_0 > 1$ *provided that*

$$\begin{aligned}
(1 - \frac{\lambda_h}{\lambda_h^*})(1 - \frac{I_{h1}\lambda_h^*}{I_{h1}^*\lambda_h}) &\geqslant 0,\\
(1 - \frac{\lambda_h}{\lambda_h^*})(1 - \frac{I_{h2}\lambda_h^*}{I_{h2}^*\lambda_h}) &\geqslant 0,\\
(1 - \frac{\lambda_m}{\lambda_m^*})(1 - \frac{I_m\lambda_m^*}{I_m^*\lambda_m}) &\geqslant 0, \ \textit{and}\\
(\frac{I_{h1}}{I_{h1}^*} - \ln\frac{I_{h1}}{I_{h1}} + \ln\frac{A_h}{A_h} + \frac{A_h}{A_h^*}) &\leqslant 0.
\end{aligned} \tag{3.8}$$

The proof of the above Theorem 3.3 is given in Appendix A1, and the Figure 2 is used to demonstrate the analytical result obtained.

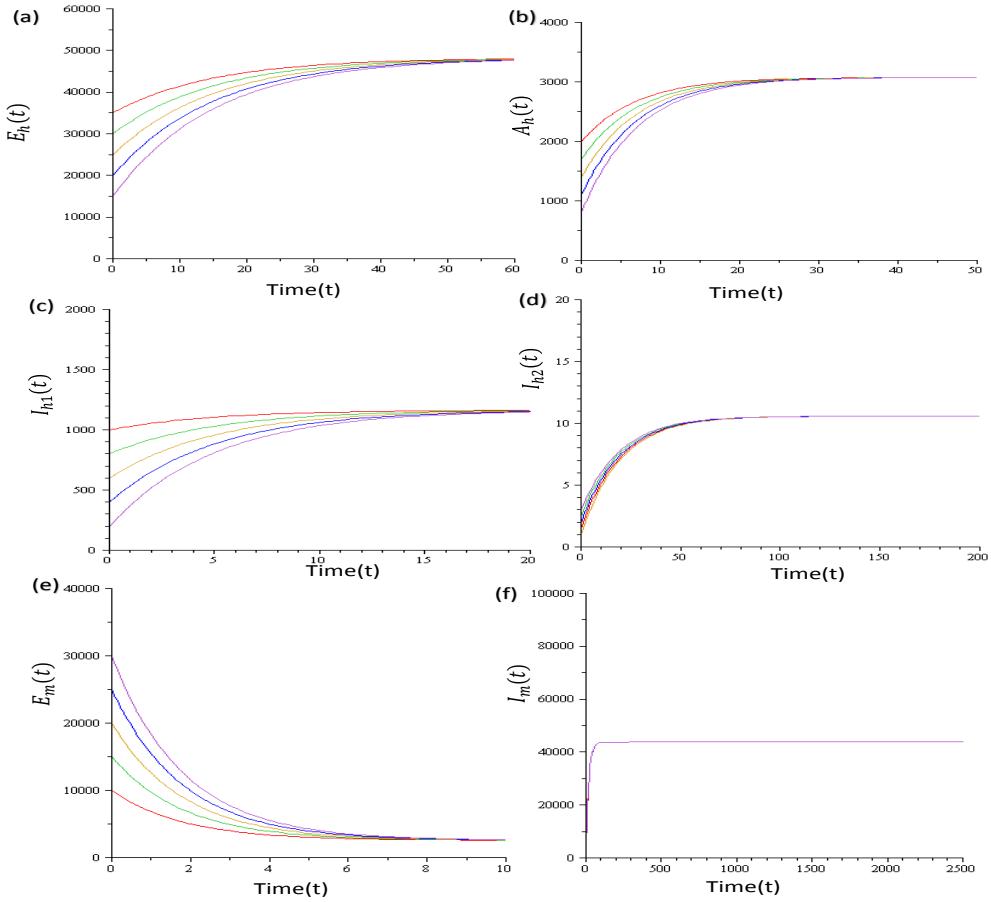

Figure 2. Time series plot of the model (2.1) with different initial conditions (represented by the different colours). The parameter values are given in the Table 3 so that $\mathcal{R}_0 = 2.178122430 > 1$; (a) the number of exposed human; (b) the number of asymptomatically infected human; (c) the number of infected human with primary clinical symptoms; (d) the number of infected human with secondary clinical symptoms; (e) the number of exposed mosquito; (f) the number of infectious mosquito.

4. Sensitivity analysis of the model (2.1)

Following the previous studies [13, 14, 34, 35], we adopted the partial ranked correlation coefficient (PRCC) for sensitivity analysis. The PRCC of the $\mathcal{R}_0$ and IAR of the model (2.1) is estimated. The sensitivity analysis results in Figure 3 suggest the top three ranked parameters (i.e., a, b and Π_m) are prioritized in controlling the DENV epidemics in Taiwan.

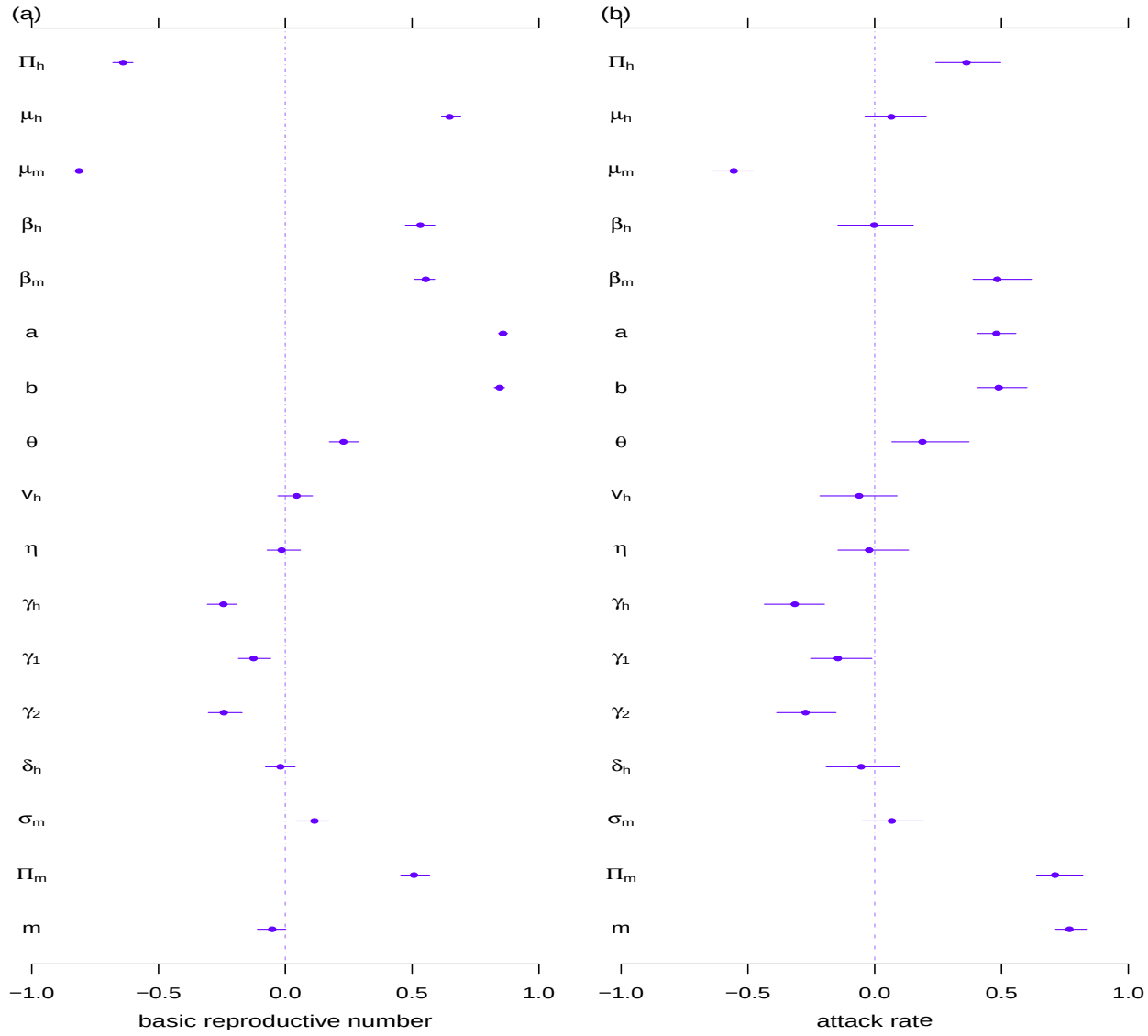

Figure 3. The partial ranked correlation coefficients (PRCC) of the model (2.1). The dots are the PRCC estimates and the bars are the 95% confidence intervals (CI). The values and ranges of the model parameters are summarized in Table 3.

5. Numerical simulations: a special case

5.1. Plug-and-play inference framework

The analyses in this section will be carried out for the special scenario of the model (2.1) in the absence of mosquito compartments (i.e., a human only sub-model). We assumed that there is no birth and death rate ($\Pi_h = \mu_h = 0$), and no disease-induced mortality rate ($\delta_h = 0$) in a short period. We also assumed that the effective contact rate of the simplified version of the model to be $\beta = \beta(t) = ab \cdot m(t)$, where $m(t)$ is the time-dependent mosquito to human ratio. This setting allows us to fit the "SIR" based model to a vector-borne disease under the "absence of vector" model structure. The term of the product of (abm) is equivalent to the standard Ross-Macdonald malaria model [36].

The equivalent (simplified) model without mosquito compartment together with the above assumptions is given by

$$\begin{aligned}
\frac{dS_h}{dt} &= -\beta I_{h_1}\frac{S_h}{N_h},\\
\frac{dE_h}{dt} &= \theta\beta I_{h_1}\frac{S_h}{N_h} - \nu_h E_h,\\
\frac{dI_{h_1}}{dt} &= \nu_h E_h - \gamma_1 I_{h_1},\\
\frac{dI_{h_2}}{dt} &= (1-\eta)\gamma_1 I_{h_1} - \gamma_2 I_{h_2},\\
\frac{dA_h}{dt} &= (1-\theta)\beta I_{h_1}\frac{S_h}{N_h} - \gamma_h A_h,\\
\frac{dR_h}{dt} &= \eta\gamma_1 I_{h_1} + \gamma_2 I_{h_2} + \gamma_h A_h,
\end{aligned} \tag{5.1}$$

where the basic reproduction ratio of the simplified model (5.1) is given by $\mathcal{R}_0(t) = \frac{\beta\theta}{\gamma_1}$.

The weekly number of cases of the i-th week is

$$Z_i = \int_{\text{week } i} \rho\gamma_1 I_{h1}\, dt, \tag{5.2}$$

where the term ρ denotes a constant reporting rate of the DENV cases. The Z_i denotes the theoretical weekly DENV cases yield from the model (5.1).

We model the observed (reported) DENV cases, C_i for the i-th week during the study period, as a partially observed Markov process (POMP, also know as hidden Markov model, HMM). Instead of implementing Poisson-distributed priors [34], all C_is are assumed to follow over-dispersed Poisson distributions according to the theoretical modelling (Eq (5.2)) outputs, Z_is. Since the rate of Poisson distribution is a Gamma random variable, the observed weekly number of people who are confirmed DENV infections (C_i of the i-th week) is a random sample from a Negative-binomial (NB) distribution. Therefore,

$$C_i \sim \text{NB}(\text{mean} = Z_i, \text{variance} = Z_i(1 + \psi Z_i)), \tag{5.3}$$

where ψ is the over-dispersion parameter for NB distribution under estimation. In this model, we set $L_i(\cdot)$ be the likelihood function for the week, which is the "probability" of C_i, given the real cases from simulations Z_i under the NB distribution [37, 38]. In this section, the model simulations are conducted by using the `R` (version 3.4.1) package "`POMP`" [39].

The overall log-likelihood, l, for the whole-time series is

$$l(\Theta) = \sum_{i=1}^{T} \ln[L_i(C_i \mid C_0, ..., C_{i-1}; \Theta)], \tag{5.4}$$

where Θ is the parameter vector under estimation. The term T denotes the total number of weeks during the study period. We apply the iterated filtering algorithm with the plug-and-play likelihood-based inference framework to estimate the maximum likelihood estimates (MLE) of Θ, (see [37, 40, 41, 42, 43, 44, 45, 46]. We use the fixed-time-step Euler-multinomial algorithm to simulate

the ODE system (5.1) [14, 34, 37, 38, 40], We compared different models using the small-sample-size corrected Akaike's Information Criterion (AICc) [44] as a measurement of the trade-off between model complexity and the goodness-of-fit. The AICc is given by

$$\text{AICc} = -2l(\hat{\Theta}) + 2k + \frac{2k(k+1)}{N-k-1}, \tag{5.5}$$

where N is the number of data points and k is the number of free parameters.

5.2. *Fitting results*

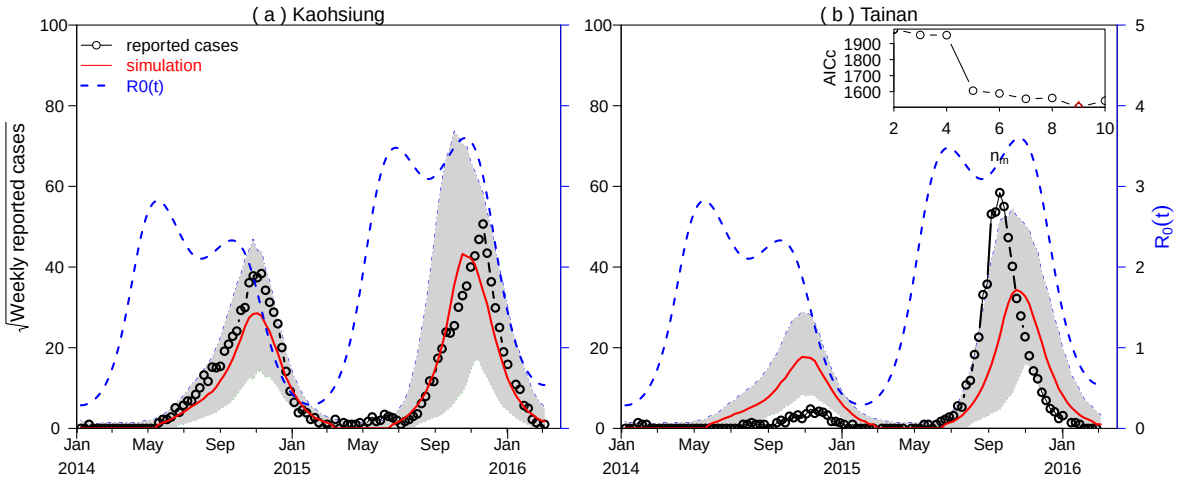

Figure 4. Fitting results of the model (5.1) using synchronized cubic spline function. The parameter estimates are summarized in Tables 3 and A1.

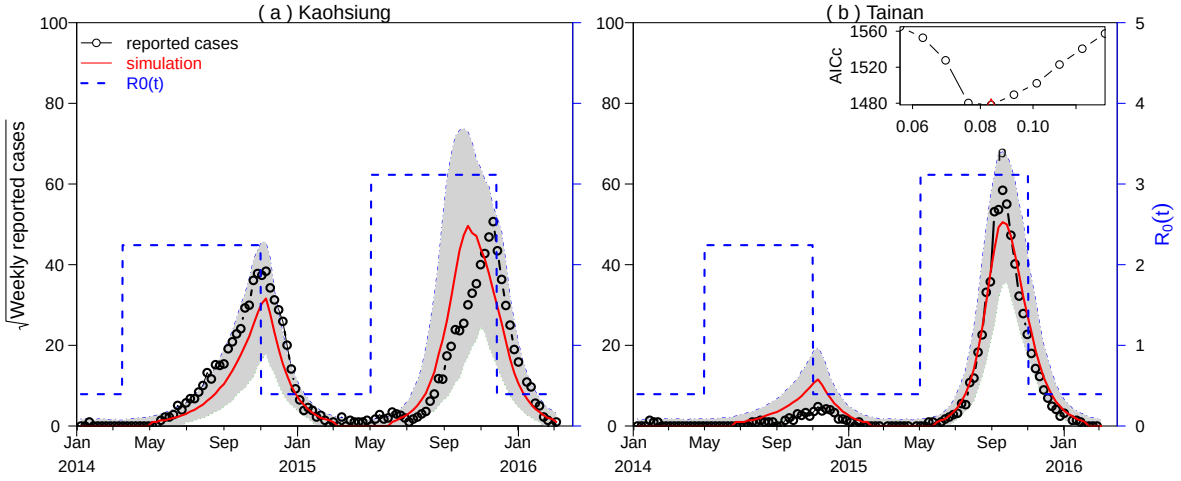

Figure 5. Fitting results of the model (5.1) using synchronized square wave function. The parameter estimates are summarized in Tables 3 and A2.

The (simplified) epidemic model (5.1) is fitted to the dengue cases time series in Kaohsiung and Tainan cities in 2014-2016. We proposed the time-dependent basic reproduction number (i.e., $\mathcal{R}_0(t)$) driven by variable mosquito abundance and dengue transmission rate (e.g., mosquito biting rate, etc). Here, we compared two numerical approaches to fit the epidemic data and reconstruct the $\mathcal{R}_0(t)$ series, namely,

- the cubic spline reconstruction approach, and
- the square wave reconstruction approach.

The cubic spline approach is defined from the previous studies [14, 47]. We used n_m to denote the number of nodes in the cubic spline of $\mathcal{R}_0(t)$ to be reconstructed. We tested different possible n_m's with the aim to find the value of n_m that leads to the lowest AICc. We further restrict that Kaohsiung and Tainan shared exactly the same cubic spline function of $\mathcal{R}_0(t)$. Hence, the two cities were fitted simultaneously with the same set of parameter estimates. For the cubic spline approach, the fitting is conducted with completely the same time series of $\mathcal{R}_0(t)$ (i.e., same timing, scale, and all settings are the same) for both cities. And we find the goodness-of-fit (in term of the MLL) can still be improved for both cities. Even though the spline can yield a relatively flexible (in term of the degree of freedom of the parameters to be estimated) $\mathcal{R}_0(t)$ reconstruction outcome, the fittings are still not satisfied. Thus, we speculate a non-synchronized $\mathcal{R}_0(t)$ would be more reasonable. The fitting results of the $\mathcal{R}_0(t)$ reconstructed by the cubic spline function are shown in Figure 4, and the parameter estimates are summarized in Table A1. The square wave is defined as a baseline transmission rate plus a constant additional value for each year. The additional values are different for both Kaohsiung and Tainan in the same year, and also vary in different years. To explore the possible non-synchronization of $\mathcal{R}_0(t)$'s in Kaohsiung and Tainan cities, we further allow the changing time of the square wave to have different estimates in the two cities. Thus, the reconstructed $\mathcal{R}_0(t)$s in Kaohsiung and Tainan are expected to have different shape which indicates that the $\mathcal{R}_0(t)$'s of the two cities are not perfectly synchronized. In Tainan, we fix the time of the occurrence of the $\mathcal{R}_0(t)$ high values (i.e., with the additional value) to be May 1 and October 31 in both 2014 and 2015. In Kaohsiung, our estimates are that the high values of $\mathcal{R}_0(t)$ occurred between March 16 and October 31 in 2014, and between May 1 and November 25 in 2015. These time shifts are crucial to achieve good fitting outcomes in Kaohsiung city. Thus, this finding indicates that the DENV outbreaks in Kaohsiung turned on early in 2014, and turned off late in 2015. For the square-wave approach, the fitting is conducted with similar series of $\mathcal{R}_0(t)$'s for the two cities. The timing (of change) and the scale of $\mathcal{R}_0(t)$'s were slightly different. Although this approach is less flexible as the spline approach (i.e., with 4 degrees of freedom decreased), it leads to better fitting results with MLL improved by 10 units. And together, the AIC improves (i.e., decreases) by 24 units. This indicates that the non-synchronized square-wave approach is a strong and significant improvement from the synchronized spline approach. The fitting results of $\mathcal{R}_0(t)$ reconstructed by the square wave function are shown in Figure 5, and the parameter estimates are summarized in Table A2. Therefore, for the spline versus square-wave approach, the non-synchronized square-wave approach has better goodness-of-fit (i.e., higher MLL) with less flexibility (i.e., less degree of freedom). In other words, the non-synchronized square-wave approach has better fitting performance (in term of the AIC). Hence, we conclude that non-synchronized $\mathcal{R}_0(t)$'s were likely to occur in the two cities.

Our (simplified) DENV epidemic model well-explained the temporal patterns of the DENV outbreaks in the two cities in Taiwan under biologically reasonable conditions (i.e., set of model parameters). We discovered that the epidemics in the two cites can be reconstructed by similar transmission

series (i.e., $\mathcal{R}_0(t)$), and also estimated with the same model structure. The square wave approach not only reduced the number of free parameters by 4, but also increased the log likelihood by 10 units. Hence, its AICc decreases roughly by 24 units from the cubic spline reconstruction, which is a significant improvement.

Although we find that the estimated transmission rates exhibited similar seasonal patterns in Kaohsiung and Tainan, they are neither completely synchronized between the two cities despite their proximity, nor periodically in-phase perfectly. If they were completely synchronized or perfectly periodic, the cubic spline approach would identify such a pattern reflected by an equivalent level of goodness-of-fit as in the square wave approach. We conclude that the time lags between the seasonal waves of the transmission rates ($\mathcal{R}_0(t)$) in the two cities are likely to occurred. Other than the pathogenic factors that can causes the phase difference in the transmissibility [48], these time lags could be due to the heterogeneity in the local conditions in Kaohsiung and Tainan cities.

6. Conclusions

We formulated and analyzed a mathematical model to study the transmission dynamics of the dengue outbreaks in Kaohsiung and Tainan cities in Taiwan in 2014–2015. We showed that the model (2.1) has two equilibria, of which the disease-free equilibrium (DFE) is locally asymptotically stable (LAS) whenever the basic reproduction number ($\mathcal{R}_0 < 1$), and unstable if the $\mathcal{R}_0 > 1$. And the endemic equilibrium (EE) is globally asymptotically stable (GAS) in the region of attraction, Ω, whenever the $\mathcal{R}_0 > 1$ (numerical examples, see Figure 2, is used to demonstrate the analytical results obtained). Our analysis shows the existence of backward bifurcation (BB) phenomenon of the model (2.1), a situation where a stable disease free-equilibrium co-exists with a stable endemic equilibrium even when the basic reproduction number ($\mathcal{R}_0$) is less than one, which makes the disease control even more difficult and is no longer dependent on the basic concept of the $\mathcal{R}_0$ (i.e., $\mathcal{R}_0 < 1$ the disease dies out in time, while $\mathcal{R}_0 > 1$ the disease persist to the community). In this paper, the analysis suggest that the backward bifurcation can be removed when the basic reproduction number is equal to one (i.e., $\mathcal{R}_0 = 1$).

We employed the plug-and-play statistical inference framework on the special case of the model (2.1) in the absence of mosquito. We fitted the simplified model (5.1) to the weekly number of cases in the Kaohsiung and Tainan Cities in Taiwan (obtained from the National Infectious Disease Statistics System [49], see Figures. 4 and 5). Our (simplified) dengue epidemic model is able to explained the temporal patterns of the dengue outbreaks in the two cities in Taiwan under biologically reasonable conditions (i.e., set of model parameters). We obtained that the epidemics in the two cites can be reconstructed by the same transmission series (i.e., $\mathcal{R}_0(t)$) and also estimated with the same model structure. This findings suggests the similarity of the dengue outbreak in a two different places during the same period of time, which could be due to the similar demographic and/or meteorological conditions. The proposed two reconstruction approaches presents (roughly) equivalent goodness-of-fit in terms of the values of the log-likelihood. However, the AICc improves (decreases) roughly by 24 units from the cubic spline to the square wave reconstruction. We also found that despite the proximity in Kaohsiung and Tainan, the estimated transmission rates were neither completely synchronized, nor periodically in-phase perfectly in the two cities. The time lags between the seasonal waves of the transmission rates in the two cities were likely to occur. These time lags could be due to the differences

in their local conditions. Furthermore, we show that the non-synchronized square-wave approach has better goodness-of-fit (i.e., higher MLL) with less flexibility (i.e., less degree of freedom). In other words, the non-synchronized square-wave approach has a better fitting performance (in term of the AIC) than the cubic spline approach. Hence, we concluded that non-synchronized $\mathcal{R}_0(t)$s were likely to occur in the two cities.

The sensitivity analysis results shows the top three ranked parameters (i.e., a, b and Π_m), that is, the mosquito biting rate, the maximum number of bites a human can receive per unit time, and the mosquito recruitment rate are the key parameters to be prioritized for controlling the Taiwan dengue outbreaks. This further suggests that proper sanitation of mosquito breeding sites and avoiding the mosquito bites are the key control measures to future dengue outbreaks in Taiwan.

List of Abbreviations

We listed the abbreviations used in Table 4.

Table 4. Summary of the abbreviations used in this work.

abbreviation	explanation / full name
AICc	corrected Akaike's Information Criterion
BB	Backward bifurcation
CI	Confidence interval
DENV	Degue virus
DENV-1	Dengue virus serotype 1
DENV-2	Dengue virus serotype 2
DENV-3	Dengue virus serotype 3
DENV-4	Dengue virus serotype 4
DFE	Disease-free equilibrium
DHF	Dengue hemorrhagic fever
DSS	Dengue shock syndrome
EE	Endemic equilibrium
EIP	Extrinsic incubation period
GAS	Globally-asymptotically stable
HMM	Hidden Markov Model
IIP	Intrinsic incubation period
LAS	Locally-asymptotically stable
MLE	Maximum likelihood estimates
MLL	Maximum log-likelihood
NB	Negative binomial (distribution)
ODE	Ordinary differential equation
POMP	partially observed Markov process
PRCC	Partial rank correlation coefficient

Acknowledgments

Zhen Jin is partly supported by Shanxi Scientific and Technology Innovation Team (201705D15111172 & 201805D131012-1). We thank reviewers for helpful comments.

Conflict of interest

The authors declare that they have no conflict of interest in this paper.

References

1. H. H. G. Silva and I. G. Silva, Influence of eggs quiescence period on the aedes aegypti (Linnaeus, 1762) (diptera, culicidae) life cycle at laboratory conditions, *Rev. Soc. Bras. Med. Trop.*, **32** (1999), 349–355.
2. C. J. McMeniman and S. L. O'Neill, A virulent wolbachia infection decreases the viability of the dengue vector aedes aegypti during periods of embryonic quiescence, *PLoS Negl. Trop. Dis.*, **4** (2010), e748.
3. H. M. Yang and C. P. Ferreira, Assessing the effects of vector control on dengue transmission, *Appl. Math. Comput.*, **198** (2008), 401–413.
4. H. M. Yang, M. L. G. Macoris, K. C. Galvani, et al., Follow up estimation of aedes aegypti entomological parameters and mathematical modellings. *Biosyst.*, **103** (2011), 360–371.
5. H. M. Yang, Assessing the influence of quiescence eggs on the dynamics of mosquito aedes aegypti, *Appl. Math.*, **5** (2014), 2696–2711.
6. S. M. Garba, A. B. Gumel and M. R. A. Bukar, Backward bifurcations in dengue transmission dynamics, *Math. Biosci.*, **215** (2008), 11–25.
7. K. S. Vannice, A. Durbin and J. Hombach, Status of vaccine research and development of vaccines for dengue, *Vaccine*, **34** (2016), 2934–2938.
8. World Health Organization, Dengue control, 2017. Available from: `http://www.who.int/denguecontrol/human/en/`.
9. S. Sang, S. Gu, P. Bi, et al., Predicting unprecedented dengue outbreak using imported cases and climatic factors in guangzhou, *PLoS Negl. Trop. Dis.*, **9** (2014), e0003808.
10. R. M. Lana, T. G. Carneiro, N. A. Honorio, et al., Seasonal and nonseasonal dynamics of aedes aegypti in Rio de Janeiro, Brazil: fitting mathematical models to trap data, *Acta Tropic.*, **129** (2014), 25–32.
11. E. P. Pliego, J. Velazquez-Castro and A. F. Collar, Seasonality on the life cycle of aedes aegypti mosquito and its statistical relation with dengue outbreaks, *Appl. Math. Model.*, **50** (2017), 484–496.
12. K. O. Okuneye, J. X. Valesco-Hernandez and A. B. Gumel, The "unholy" chikungunya-dengue-zika trinity: a theoretical analysis, *J. Biol. Syst.*, **25** (2017), 587–603.
13. D. Gao, Y. Lou, D. He, et al., Prevention and control of zika as a mosquito-borne and sexually transmitted disease: a mathematical modeling analysis, *Sci. Rep.*, **6** (2016), 28070.

14. S. Zhao, L. Stone, D. Gao, et al., Modelling the large-scale yellow fever outbreak in Luanda, Angola, and the impact of vaccination, *PLoS Negl. Trop. Dis.*, **12** (2018), e0006158.
15. P. Guo, T. Liu, Q. Zhang, et al., Developing a dengue forecast model using machine learning: a case study in China, *PLoS Negl. Trop. Dis.*, **11** (2017), e0005973.
16. T. P. O. Evans and S. R. Bishop, A spatial model with pulsed releases to compare strategies for the sterile insect technique applied to the mosquito Aedes aegypti, *Math. Biosci.*, **254** (2014), 6–27.
17. R. R. Mahale, A. Mehta, A. K. Shankar, et al., Delayed subdural hematoma after recovery from dengue shock syndrome, *J. Neurosci. Rural Pract.*, **7** (2016), 323–324.
18. D. J. Gubler, E. E. Ooi, S. G. Vasudevan, et al., *Dengue and dengue hemorrhagic fever*, 2nd ed. Wallingford, UK: CAB International, 2014.
19. S. F. Wang, W. H. Wang, K. Chang, et al., Severe dengue fever outbreak in Taiwan, *Am. J. Trop. Med. Hyg.*, **94** (2016), 193–197.
20. M. Chan and M. A. Johansson, The incubation periods of dengue viruses, *PLoS One*, **7** (2012), e50972.
21. C. A. Manore, K. S. Hickman, S. Xu, et al., Comparing dengue and chikungunya emergence and endemic transmission in A. egypti and A.albopictus, *J. Theor. Bio.*, **356** (2014), 174–191.
22. Sanofi Pasteur, First Dengue Vaccine Approved in More than 10 Countries by Sanofi Pasteur, 2019. Available from: `https://www.sanofipasteur.com/en/`.
23. World Health Organization, Updated Questions and Answers related to information presented in the Sanofi Pasteur press release on 30 November 2017 with regards to the dengue vaccine Dengvaxia, 2019. Available from: `https://www.who.int/immunization/diseases/dengue/q_and_a_dengue_vaccine_dengvaxia/en/`.
24. H. M. Yang, M. L. G. Macoris, K. C. Galvani, et al., Assessing the effects of temperature on the population of Aedes aegypti, the vector of dengue, *Epidemiol. Infect.*, **137** (2009), 1188–1202.
25. H. M. Yang, M. L. G. Macoris, K. C. Galvani, et al., Assessing the effects of temperature on dengue transmission, *Epidemiol. Infect.*, **137** (2009), 1179–1187.
26. A. B. Gumel, Causes of backward bifurcations in some epidemiological models, *J. Math. Anal. Appl.*, **395** (2012), 355–365.
27. K. Okuneye and A. B. Gumel, Analysis of a temperature- and rainfall-dependent model for malaria transmission dynamics, *Mathe. Biosci.*, **287** (2017), 72–92.
28. N. Hussaini, K. Okuneye and A. B. Gumel, Mathematical analysis of a model for zoonotic visceral leishmaniasis, *Infect. Dis. Model.*, **2** (2017), 455–474.
29. S. Usaini, U. T. Mustapha and S. S. Musa, Modelling scholastic underachievement as a contagious disease, *Math. Meth. Appl. Sci.*, **41** (2018), 8603–8612.
30. P. van den Driessche and J. Watmough, Reproduction numbers and sub-threshold endemic equilibria for compartmental models of disease transmission, *Math. Biosci.*, **180** (2002), 29–48.
31. T. P. Endy, S. Chunsuttiwat, A. Nisalak, et al., Epidemiology of inapparent and symptomatic acute dengue virus infection: a prospective study of primary school children in Kamphaeng Phet, Thailand, *Amer. J. Epi.*, **156** (2002), 40–51.

32. M. J. P. Poirier, D. M. Moss, K. R. Feeser, et al., Measuring Haitian children's exposure to chikungunya, dengue and malaria, *Bull World Health Organ.*, **94** (2016), 817–825.
33. C. H. Chen, Y. C. Huang and K. C. Kuo, Clinical features and dynamic ordinary laboratory tests differentiating dengue fever from other febrile illnesses in children, *J. Microb. Immunol. Infect.*, **51** (2018), 614–620.
34. S. Zhao, Y. Lou, A. P. Chiu, et al., Modelling the skip-and-resurgence of Japanese encephalitis epidemics in Hong Kong, *J. Theor. Biol.*, **454** (2018), 1–10.
35. Y. Xiao, S. Tang and J. Wu, Media impact switching surface during an infectious disease outbreak, *Scient. Rep.*, **5** (2015), 7838.
36. D. L. Smith, K. E. Battle, S. I. Hay, et al., Ross, Macdonald, and a theory for the dynamics and control of mosquito-transmitted pathogens, *PLoS Pathog.*, **8** (2012), e1002588.
37. Q. Lin, Z. Lin, A. P. Y. Chiu, et al., Seasonality of influenza A(H7N9) virus in China -fitting simple epidemic models to human cases, *PLoS One*, **11** (2016), e0151333.
38. C. Breto, D. He, E. L. Ionides , et al., Time series analysis via mechanistic models, *Ann. Appl. Stat.*, **3** (2009), 319–348.
39. The website of `R` package "`pomp`": statistical inference for partially-observed Markov processes, 2018. Available from: `https://kingaa.github.io/pomp/`.
40. D. He, R. Lui, L. Wang, et al., Global Spatio-temporal Patterns of influenza in the post-pandemic era, *Sci Rep.*, **5** (2015), 11013.
41. E. L. Ionides, C. Breto and A. A. King, Inference for nonlinear dynamical systems, *Proc. Natl. Acad. Sci.*, **103** (2006), 18438–18443.
42. E. L. Ionides, A. Bhadra, Y. Atchade, et al., Iterated filtering, *Ann. Stat.*, **39** (2011), 1776–1802.
43. D. J. Earn, D. He, M. B. Loeb, et al., Effects of school closure on incidence of pandemic influenza in Alberta, Canada, *Ann. Intern. Med.*, **156** (2012), 173–181.
44. A. Camacho, S. Ballesteros, A. L. Graham, et al., Explaining rapid reinfections in multiple-wave influenza outbreaks: Tristan da Cunha 1971 epidemic as a case study, *Proc. Biol. Sci.*, **278** (2011), 3635–3643.
45. D. He, J. Dushoff, T. Day, et al., Mechanistic modelling of the three waves of the 1918 influenza pandemic, *Theory Ecol.*, **4** (2011), 283–288.
46. D. He, E. L. Ionides and A. A. King, Plug-and-play inference for disease dynamics: measles in large and small populations as a case study, *J. R. Soc. Interf.*, **7** (2010), 271–283.
47. D. He, D. Gao, Y. Lou, et al., A comparison study of zika virus outbreaks in French Polynesia, Colombia and the state of Bahia in Brazil, *Sci. Rep.*, **7** (2017), 273.
48. S. Zhao, S. S. Musa, J. Qin , et al., Phase-shifting of the transmissibility of macrolide-sensitive and resistant Mycoplasma pneumoniae epidemics in Hong Kong, from 2015 to 2018, *Int. J. Infect. Dis.*, **81** (2019), 251–253.
49. Taiwan National Infectious Disease Statistics System, Dengue, 2018. Available from: `https://nidss.cdc.gov.tw/en/Default.aspx?op=4`.

50. C. Yang, X. Wang, D. Gao , et al., Impact of awareness programs on cholera dynamics: two modeling approaches, *Bull. Math. Biol.*, **79** (2017), 2109–2131.

51. G. Sun, J. Xie, S. Huang, et al., Transmission dynamics of cholera: mathematical modeling and control strategies, *Commun. Non. Sci. Numer. Simulat.*, **45** (2017), 235–244.

52. J. P. LaSalle, The stability of dynamical systems, Regional Conference Series in Applied Mathematics, Soceity for industrial and Applied Mathematics, Philadelphia, 1976.

53. D. S. Shepard, Y. A. Halasa, B. K. Tyagi, et al., Economic and disease burden of dengue illness in India, *Am. J. Trop. Med. Hyg.*, **91** (2014), 1235–1242.

54. N. T. Toan, S. Rossi, G. Prisco, et al., Dengue epidemiology in selected endemic countries: factors influencing expansion factors as estimates of underreporting, *Trop. Med. Int. Health.*, **20** (2015), 840–863.

55. E. Sarti, M. L'Azou, M. Mercado, et al., A comparative study on active and passive epidemiological surveillance for dengue in five countries of Latin America, *Int. J. Infect. Dis.*, **44** (2016), 44–49.

Appendices

A1. The proof of theorem 3.3

Proof. Define a Lyapunov function as follows

$$\begin{aligned} V(t) =& J_1(S_h - S_h^* - S_h^* \ln \frac{S_h}{S_h^*}) + J_2(E_h - E_h^* - E_h^* \ln \frac{E_h}{E_h^*}) + J_3(A_h - A_h^* - A_h^* \ln \frac{A_h}{A_h^*}) + \\ & J_4(I_{h_1} - I_{h_1}^* - I_{h_1}^* \ln \frac{I_{h_1}}{I_{h_1}^*}) + J_5(I_{h_2} - I_{h_2}^* - I_{h_2}^* \ln \frac{I_{h_2}}{I_{h_2}^*}) + K_1(S_m - S_m^* - S_m^* \ln \frac{S_m}{S_m^*}) + \\ & K_2(E_m - E_m^* - E_m^* \ln \frac{E_m}{E_m^*}) + K_3(I_m - I_m^* - I_m^* \ln \frac{I_m}{I_m^*}), \end{aligned} \tag{A1-1}$$

where $J_1 = 2$, $J_2 = \frac{1}{1-\theta}$, $J_3 = \frac{1}{(\theta)}$, $J_4 = \frac{\lambda_h^* S_h^*}{\nu_h E_h^*}$, $J_5 = \frac{\lambda_h^* S_h^*}{(1-\eta)\gamma_1 I_{h1}^*}$, $K_1 = K_2 = 1$, and $K_3 = \frac{\lambda_m^* S_m^*}{\sigma_m E_m^*}$.
Thus, the Lyapunov derivative computed along solutions of the system (2.1) is given by

$$\begin{aligned} \dot{V}(t) =& J_1(1 - \frac{S_h^*}{S_h})\dot{S_h} + J_2(1 - \frac{A_h^*}{A_h})\dot{A_h} + J_3(1 - \frac{E_h^*}{E_h})\dot{E_h} + J_4(1 - \frac{I_{h_1}^*}{I_{h_1}})\dot{I_{h_1}} + \\ & J_5(1 - \frac{I_{h_2}^*}{I_{h_2}})\dot{I_{h_2}} + K_1(1 - \frac{S_m^*}{S_m})\dot{S_m} + K_2(1 - \frac{E_m^*}{E_m})\dot{E_m} + K_3(1 - \frac{I_m^*}{I_m})\dot{I_m}. \end{aligned} \tag{A1-2}$$

Hence,

$$
\begin{aligned}
\dot{V}(t) = & - J_1 \frac{\mu_h (S_h - S_h^*)^2}{S_h} + \\
& J_1 \lambda_h^* S_h^* [1 - \frac{\lambda_h S_h}{\lambda_h^* S_h^*} - \frac{S_h^*}{S_h} + \frac{\lambda_h}{\lambda_h^*}] + \\
& J_2 (1-\theta) \lambda_h^* S_h^* [\frac{\lambda_h S_h}{\lambda_h^* S_h^*} - \frac{A_h}{A_h^*} - \frac{A_h^* \lambda_h S_h}{A_h \lambda_h^* S_h^*} + 1] + \\
& J_3 \theta \lambda_h^* S_h^* [\frac{\lambda_h S_h}{\lambda_h^* S_h^*} - \frac{E_h}{E_h^*} - \frac{E_h^* \lambda_h S_h}{E_h \lambda_h^* S_h^*} + 1] + \\
& J_4 v_h E_m^* [\frac{E_h}{E_h^*} - \frac{I_{h1}}{I_{h1}^*} - \frac{I_{h1}^* E_h}{I_{h1} E_h^*} + 1] + \\
& J_5 (1-\eta) \gamma_1 I_h h1^* [\frac{I_{h1}}{I_{h1}^*} - \frac{I_{h2}}{I_{h2}^*} - \frac{I_{h2}^* I_{h1}}{I_{h2} I_{h1}^*} + 1] + \\
& - K_1 \frac{\mu_m (S_m - S_m^*)^2}{S_m} + \\
& K_1 \lambda_m^* S_m^* [1 - \frac{\lambda_m S_m}{\lambda_m^* S_m^*} - \frac{S_m^*}{S_m} + \frac{\lambda_m}{\lambda_m^*}] + \\
& K_2 \lambda_m^* S_m^* [\frac{\lambda_m S_m}{\lambda_m^* S_m^*} - \frac{E_m}{E_m^*} - \frac{E_m^* \lambda_m S_m}{E_m \lambda_m^* S_m^*} + 1] + \\
& K_3 \sigma_m E_m^* [\frac{E_m}{E_m^*} - \frac{I_m}{I_m^*} - \frac{I_m^* E_m}{I_m E_m^*} + 1].
\end{aligned} \tag{A1-3}
$$

Following [50, 51], the function $v(x) = 1 - x + \ln x$, if $x > 0$, it leads to $v(x) \leqslant 0$. And if $x = 1$, we have $v(x) = 0$. Thus, $x - 1 \geqslant \ln(x)$ for any $x > 0$. Then, we also have that

$$
\begin{aligned}
& \lambda_h^* S_h^* [2 - \frac{S_h^*}{S_h} - \frac{E_h}{E_h^*} - \frac{\lambda_h S_h E_h^*}{\lambda_h^* S_h^* E_h} + \frac{\lambda_h}{\lambda_h^*}] \\
& = \lambda_h^* S_h^* [-(1 - \frac{\lambda_h}{\lambda_h^*})(1 - \frac{I_{h1} \lambda_h^*}{I^* \lambda_h}) + 3 - \frac{S_h^*}{S_h} - \frac{\lambda_h S_h E_h^*}{\lambda_h^* S_h^* E_h} - \frac{I_{h1} \lambda^*}{I_{h1}^* \lambda_h} - \frac{E_h}{E_h^*} + \frac{I_{h1}}{I_{h1}^*}] \\
& \leqslant \lambda_h^* S_h^* [-(\frac{S_h^*}{S_h} - 1) - (\frac{\lambda_h S_h E_h^*}{\lambda_h^* S_h^* E_h} - 1) - (\frac{I_{h1} \lambda_h^*}{I_{h1}^* \lambda_{h1}} - 1) - \frac{E_h}{E_h^*} + \frac{I_{h1}}{I_{h1}^*}] \\
& \leqslant \lambda_h^* S_h^* [-\ln(\frac{S_h^*}{S_h} \frac{\lambda_h S_h E_h^*}{\lambda^* S_h^* E_h} \frac{I_{h1} \lambda_h^*}{I_{h1}^* \lambda_h}) - \frac{E_h}{E_h^*} + \frac{I_{h1}}{I_{h1}^*}] \\
& = \lambda_h^* S_h^* [\frac{I_{h1}}{I_{h1}^*} - \ln(\frac{I_{h1}}{I_{h1}^*}) + \ln(\frac{E_h}{E_h^*}) - \frac{E_h}{E_h^*}].
\end{aligned} \tag{A1-4}
$$

Similarly, we have

$$
\lambda_h^* S_h^* [2 - \frac{S_h^*}{S_h} - \frac{A_h}{A_h^*} - \frac{\lambda_h S_h A_h^*}{\lambda_h^* S_h^* A_h} + \frac{\lambda_h}{\lambda_h^*}] \leqslant \lambda_h^* S_h^* [\frac{I_{h2}}{I_{h2}^*} - \ln(\frac{I_{h2}}{I_{h2}^*}) + \ln(\frac{A_h}{A_h^*}) - \frac{A_h}{A_h^*}], \tag{A1-5}
$$

and

$$\lambda_m^* S_m^* [2 - \frac{S_m^*}{S_m} - \frac{E_m}{E_m^*} - \frac{\lambda_m S_m E_m^*}{\lambda_m^* S_m^* E_m} + \frac{\lambda_m}{\lambda_m^*}] \leqslant \lambda_m^* S_m^* [\frac{I_m}{I_m^*} - \ln(\frac{I_m}{I_m^*}) + \ln(\frac{E_m}{E_m^*}) - \frac{E_m}{E_m^*}]. \tag{A1-6}$$

Furthermore, we have that

$$\lambda_h^* S_h^* (\frac{E_h}{E_h^*} - \frac{I_{h1}}{I_{h1}^*} - \frac{I_{h1}^* E_h}{I_{h1} E_h^*} + 1) \leqslant \lambda_h^* S_h^* (\frac{E_h}{E_h^*} - \ln(\frac{E_h}{E_h^*}) + \ln(\frac{I_{h1}}{I_{h1}^*}) - \frac{I_{h1}}{I_{h1}^*}), \tag{A1-7}$$

and also

$$\lambda_h^* S_h^* (\frac{I_{h1}}{I_{h1}^*} - \frac{I_{h2}}{I_{h2}^*} - \frac{I_{h2}^* I_{h1}}{I_{h2} I_{h1}^*} + 1) \leqslant \lambda_h^* S_h^* (\frac{I_{h1}}{I_{h1}^*} - \ln(\frac{I_{h1}}{I_{h1}^*}) + \ln(\frac{I_{h2}}{I_{h2}^*}) - \frac{I_{h2}}{I_{h2}^*}), \tag{A1-8}$$

as well as

$$\lambda_m^* S_m^* (\frac{E_m}{E_m^*} - \frac{I_m}{I_m^*} - \frac{I_m^* E_m}{I_m E_m^*} + 1) \leqslant \lambda_m^* S_m^* (\frac{E_m}{E_m^*} - \ln(\frac{E_m}{E_m^*}) + \ln(\frac{I_m}{I_m^*}) - \frac{I_m}{I_m^*}). \tag{A1-9}$$

Hence, the equations (A1-1)-(A1-9) together with condition (3.8) ensure that $\frac{dV}{dt} \leqslant 0$. Furthermore, the strict inequality $\frac{dV}{dt} = 0$ holds only for $S_h = S_h^*$, $E_h = E_h^*$, $A_h = A_h^*$, $I_{h_1} = I_{h_1}^*$, $I_{h_2} = I_{h_2}^*$, $R_h = R_h^*$, $S_m = S_m^*$ $E_m = E_m^*$ and $I_m = I_m^*$. Thus, the endemic equilibrium state E^* is the only positive invariant set to the system (2.1) contained entirely in $\Big\{(S_h, E_h, A_h, I_{h_1}, I_{h_2}, R_h, S_m, E_m, I_m) \in \Omega : S_h = S_h^*, E_h = E_h^*, A_h = A_h^*, I_{h_1} = I_{h_1}^*, I_{h_2} = I_{h_2}^*, R_h = R_h^*, S_m = S_m^*, E_m = E_m^*, I_m = I_m^*\Big\}$. Therefore, it follows from the LaSalle's invariance principle [52] that every solutions to the equations in (A1-2) with initial conditions in Ω converge to stable endemic equilibrium point, E^*, as $t \to \infty$. Hence, the positive endemic equilibrium is globally asymptotically stable. □

A2. Summary table of initial state values and parameters estimation results of the model (5.1)

Table A1. Summary table of initial state values and parameters estimation results of the model (5.1) with **cubic spline** function.

Parameter	Value (Kaohsiung)	Value (Tainan)	Source
$S_h(0)$	0.93212	0.8774	estimated
$E_h(0)$	3.229552×10^{-6}	3.241949×10^{-6}	estimated
$A_h(0)$	3.229552×10^{-6}	3.241949×10^{-6}	estimated
$I_{h_1}(0)$	3.229552×10^{-6}	3.241949×10^{-6}	estimated
$I_{h_1}(0)$	3.229552×10^{-6}	3.241949×10^{-6}	estimated
$R_h(0)$	0.0688	0.1226	estimated
β	1×10^{-20}	1×10^{-20}	estimated
ρ	0.0631	0.0631	[53, 54, 55]
n_m	9	9	estimated

Table A2. Summary table of initial state values and parameters estimation results of the model (5.1) with the **square wave** function.

Parameter	Value (Kaohsiung)	Value (Tainan)	Source
$S_h(0)$	0.9483	0.9161	estimated
$E_h(0)$	2.773339×10^{-6}	3.24338×10^{-6}	estimated
$A_h(0)$	2.773339×10^{-6}	3.24338×10^{-6}	estimated
$I_{h_1}(0)$	2.773339×10^{-6}	3.24338×10^{-6}	estimated
$I_{h_1}(0)$	2.773339×10^{-6}	3.24338×10^{-6}	estimated
$R_h(0)$	0.0517	0.0839	estimated
β	1.9986	1.9986	estimated
ρ	0.0837	0.0837	estimated

AIMS Press